

Associated Production of a Top Quark and a Charged Higgs Boson

Edmond L. Berger^{1*}, Tao Han^{2†}, Jing Jiang^{1‡}, Tilman Plehn^{3§}¹*High Energy Physics Division, Argonne National Laboratory, Argonne, IL 60439*²*Department of Physics, University of Wisconsin, Madison, WI 53706 and*³*CERN Theory Group, CH-1211 Geneva 23, Switzerland*

(Dated: November 8, 2018)

We compute the inclusive and differential cross sections for the associated production of a top quark along with a charged Higgs boson at hadron colliders to next-to-leading order (NLO) in perturbative quantum chromodynamics (QCD) and in supersymmetric QCD. For small Higgs boson masses we include top quark pair production diagrams with subsequent top quark decay into a bottom quark and a charged Higgs boson. We compare the NLO differential cross sections obtained in the bottom parton picture with those for the gluon-initiated process and find good agreement. The effects of supersymmetric loop contributions are explored; only the corrections to the Yukawa coupling are sizable in the potential discovery region at the LHC. All expressions and numerical results are fully differential, permitting selections on the momenta of both the top quark and the charged Higgs boson.

PACS numbers: 14.80.Cp, 13.85.Qk

I. INTRODUCTION

The elucidation of electroweak symmetry breaking is an important goal of particle physics. In the standard model, one neutral scalar Higgs boson is assumed to exist, and it is associated with the generation of the masses of the electroweak gauge bosons, as well as of the fermions. The Higgs boson has not yet been observed, and direct searches place a lower limit of about 114 GeV on its mass [1]. Extensions of the standard model include the possibility of more Higgs fields. Its minimal supersymmetric extension MSSM requires two doublets to give mass to up-type and down-type fermions and to cancel anomalies. They yield five physical Higgs bosons: two neutral CP-even states, a CP-odd state, and a pair of charged scalars. At lowest order in perturbation theory, their masses and couplings depend on two parameters which may be chosen as the pseudoscalar mass m_A and the ratio of the two vacuum-expectation values $\tan\beta = v_2/v_1$. Comprehensive analyses have been performed to establish the coverage of the $(\tan\beta, m_A)$ parameter space at the CERN Large Hadron Collider (LHC) [2]. While the observation of at least one of the two CP even Higgs bosons may not pose a problem for the LHC [3], it will be challenging to distinguish it from its standard model counterpart over a large fraction of the parameter space. For small values of $\tan\beta$ the only viable channel to observe a heavy Higgs boson could be the resonant production of the scalar H with subsequent decay to $hh \rightarrow b\bar{b}\gamma\gamma$ [4]. For large values of $\tan\beta$, the identification of a charged Higgs boson would provide evidence for a Higgs sector beyond the standard model, meaning at least two Higgs doublets, and possibly a supersymmetric Higgs sector.

If the charged Higgs boson is lighter than the top quark, there is a good chance that it will be discovered via the new decay channel $t \rightarrow bH^+$ at the Tevatron (2 TeV in $p\bar{p}$ collisions) or at the LHC (14 TeV with pp collisions). Searches have been conducted by the CDF and D0 collaborations using Run I data at the Tevatron [5], and significant bounds on the mass m_H and $\tan\beta$ have been derived. If the charged Higgs boson is heavier than the top quark, then its observation at hadron colliders becomes more challenging. In particular, there are no tree level couplings of a single charged Higgs boson to gauge boson pairs and thus the production of H^\pm in weak boson fusion is inaccessible. The cross section for H^+H^- pair production is likely to be too small, and the heavy quark backgrounds may be too large for the observation of charged Higgs boson pairs, unless additional supersymmetric particles enhance this loop-induced rate [6, 7]. The situation in the associated production of a charged Higgs boson with a W boson is similar. The standard model leads to a fairly small rate, but supersymmetric particle loops might enhance the rate considerably [8, 9].

The most promising search channel known for a heavy H^\pm is the associated production of a top quark and the charged Higgs boson $pp \rightarrow tH^- + X$ [10]. There are advanced detector studies available for both $H^- \rightarrow \bar{t}b$ [11] and $H^- \rightarrow \tau\bar{\nu}$ [12] decays based this production process. The advantage in this channel is that the Yukawa coupling to a top quark and a bottom quark is enhanced by a power of $\tan\beta$ for large values of $\tan\beta$, just like the bottom quark Yukawa couplings of the heavy neutral Higgs bosons. The production cross section can be evaluated with or without integration over the final state bottom quark phase

* berger@anl.gov

† than@pheno.physics.wisc.edu

‡ jiangj@hep.anl.gov

§ tilman.plehn@cern.ch

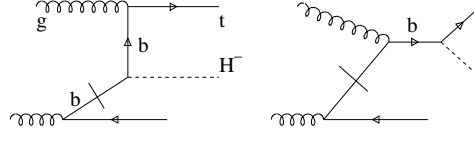


Figure 1: The leading order Feynman diagrams for the production process $gb \rightarrow tH^-$. We indicate how the bottom partons are created through gluon splitting.

space, corresponding to ignoring or observing the final state bottom quark experimentally. Here and henceforth, we use the term ‘exclusive’ to refer to measurement with the final state bottom quark observed and ‘inclusive’ to refer to that with the final state bottom quark ignored.

The total rate for the process $pp \rightarrow \bar{b}tH^- + X$ receives large corrections from collinear logarithms, originating from the radiation of a forward bottom quark jet [13, 14]. These logarithms can be resummed to all orders in the strong coupling strength α_s , leading to the bottom parton picture [13] with an appropriate bottom quark factorization scale [14, 15, 16]. This resummation of large collinear logarithms is valid not only for charged Higgs boson production, but it is generic as long as there is a large mass scale M leading to $\log(M/p_{T,b})$; in our case $M = m_t + m_H$. In the case of neutral Higgs boson production the comparison of higher order predictions for total cross sections shows impressive agreement between exclusive gluon-initiated and inclusive bottom parton results [17, 18], although the absence of a heavy scale in neutral Higgs boson production in association with bottom quarks might impact some final state distributions. Thus, one may consider the leading order subprocess as

$$gb \rightarrow tH^-. \quad (1)$$

Note that there is an analogous charge-conjugate subprocess $\bar{g}\bar{b} \rightarrow \bar{t}H^+$, but throughout this paper we will present results only for the channel in Eq. (1), unless stated otherwise. The effect of including the charge-conjugate channel is merely a factor of two increase in all rates. Calculations of the next-to-leading order (NLO) total cross section are available in perturbative quantum chromodynamics (QCD) [14, 19] as well as in supersymmetric QCD [14]. The inclusion of these NLO contributions to the inclusive gb initial state process consistently merges the inclusive process $gb \rightarrow tH^-$ with the exclusive process $gg \rightarrow \bar{b}tH^-$, which now appears as part of the set of NLO diagrams. Moreover, the NLO contributions increase the reliability of the theoretical predictions by reducing the scale dependence of the total rate.

In this paper, we present fully differential NLO cross sections for the process $gb \rightarrow tH^-$. The differential distributions are desirable, as are predictions of expected correlations among the final state observables, since selections on final state kinematic variables must be made in experimental studies, for reasons of event acceptance and background rejection. In Sec. II, we outline the phase-space slicing method which we adopt. We then study the NLO production rates at the LHC and the Tevatron with the associated theoretical uncertainties. We present the typical kinematic distributions in Sec. III. For searches in the framework of the MSSM we perform a systematic study of the effect of leading and sub-leading supersymmetric QCD corrections on the rate in Sec. IV. Conclusions are summarized in Sec. V.

II. NEXT-TO-LEADING ORDER QCD CORRECTIONS

Before presenting our calculation, we first lay out our conventions. Throughout the paper we use running couplings α_s, y_b, y_t consistent with the order of perturbation theory, *i.e.* one-loop running for the leading order and two-loop running for the next-to-leading order results. If not explicitly stated otherwise we neglect the bottom quark mass m_b in the phase space as well as in the matrix elements, while naturally keeping it in the Yukawa coupling. The Yukawa coupling is normalized to $m_b(m_b) = 4.2$ GeV and a pole mass of 4.6 GeV. Moreover, we use the respective CTEQ5 parton densities [20]. We refer frequently to the K factor defined by $K = \sigma_{\text{NLO}}/\sigma_{\text{LO}}$ to indicate the NLO QCD correction over the leading order cross section. The default choices of the renormalization scale and the factorization scale are taken to be proportional to the hard scale in the process [14, 15]

$$\mu_R^0 = M/2 \quad \mu_F^0 = M/5 \quad (M = m_H + m_t). \quad (2)$$

At leading order in QCD we start from the parton-level production process as in Eq. (1), with the diagrams depicted in Fig. 1. It is appropriate to define the bottom quark as a parton at high energies since the DGLAP evolution resums large logarithms $\log p_{T,b}$ from small $p_{T,b}^{\text{min}} \sim m_b$ to a maximum value $p_{T,b}^{\text{max}}$ (which in turn determines the b -quark factorization scale). The bottom parton density is therefore not suppressed by a simple power of α_s . The leading order cross section for a process involving one incoming bottom parton and an incoming gluon is of the order $\alpha_s y_{b,t}^2$, where $y_{b,t}$ is the bottom-top-Higgs Yukawa

coupling. If $y_{b,t}$ is written as $y_{b,t} = y_t + y_b$, y_t and y_b are the terms proportional to m_t and m_b respectively. For large values of $\tan \beta$, $y_{b,t}$ is dominated by y_b , which is multiplied by $\tan \beta$. The validity of our choice of the process in Eq. (1) as the leading contribution is confirmed by our numerical results, namely that the perturbative series is well behaved over a wide range of scales.

There are two classes of NLO contributions:

- (1) Virtual gluon exchange corrections to the lowest order process and the corresponding real gluon emission corrections, both of order $\alpha_s^2 y_{b,t}^2$,

$$\begin{aligned} gb &\rightarrow tH^- && \text{(virtual correction)} \\ gb &\rightarrow tH^- g. \end{aligned} \tag{3}$$

- (2) The purely gluon-initiated and the purely quark-initiated diagrams, which lead to cross sections also of the order $\alpha_s^2 y_{b,t}^2$,

$$\begin{aligned} gg, q\bar{q}, b\bar{b} &\rightarrow tH^- \bar{b}, & bb &\rightarrow tH^- b, \\ b\bar{q} &\rightarrow tH^- \bar{q}, & bq &\rightarrow tH^- q. \end{aligned} \tag{4}$$

Because we neglect the bottom quark mass in the phase space and in the matrix elements, the purely gluon and purely quark initiated subprocesses are divergent in the collinear limit. In our calculation these divergences are removed through mass factorization, *i.e.* the proper definition of all parton densities to NLO.

One may think about an alternative treatment of the associated production process, namely not to take the b quarks as partons, but rather to start with the process $gg \rightarrow tH^- \bar{b}$ as the leading contribution at the LHC. These exclusive diagrams are part of the α_s correction to the inclusive bottom–gluon fusion process. For a choice of the factorization scale $\mu_F \rightarrow m_b$ the bottom parton density vanishes, in contrast to the gluon density, which is stable and well defined down to scales of the order of Λ_{QCD} . In a physical picture we then consistently switch off all large collinear logarithms, because we have identified $p_{T,b}^{\text{max}} \equiv \mu_{F,b}$. In this limit we are left only with the purely light-flavor $q\bar{q}$ and gg induced processes listed in Eq. (4). We will use this limit of a small bottom quark factorization scale in Sec. III, to check the impact of the bottom parton picture on the differential cross sections with respect to the heavy final state kinematics.

A. Phase-space slicing

One of the main tasks of our calculation is to integrate the three-body matrix elements over the phase space of the unobserved particle in the final state. The situation is different from the case of single particle inclusive production because we wish to retain control over the kinematic variables of the second particle in the final state, while at the same time integrating over enough of the phase space to ensure cancellation of all infrared and collinear divergences. For these purposes, several techniques have been introduced. The phase-space slicing [21, 22] and the subtraction methods [23] are two ways to extract the singularities in the real emission contributions as exclusively as possible. All relevant information needed to compute a $2 \rightarrow 2$ particle NLO cross section using the two–cutoff slicing method is nicely compiled in Ref. [22]. We follow this description closely in our calculations.

The ultraviolet divergences arising in the virtual $2 \rightarrow 2$ corrections are regularized using dimensional regularization. The heavy final state masses are renormalized in the on-shell scheme, while all couplings — the strong coupling as well as the bottom quark and the top quark Yukawa couplings — are renormalized in the $\overline{\text{MS}}$ scheme. The mismatch of the pre-factors between the virtual corrections and the counter terms leads to the usual explicit $\log \mu_R$ dependence of the NLO cross section on the renormalization scale.

Virtual gluon exchange and real parton emission lead to both infrared and collinear divergences, which are partially canceled with each other and partially removed through mass factorization, *i.e.* the consistent definition of parton densities. The situation is relatively simple for processes with initial states which are different from the leading order one gb , because no infrared divergence appears. Schematically we can write the contributions arising from the processes given in Eq. (4) as:

$$d\sigma_q = d\sigma_{2 \rightarrow 3,q}^{\text{HC}} + d\sigma_{2 \rightarrow 3,q}^{\text{finite}} + d\sigma_q^{\text{HMF}}. \tag{5}$$

The label HC indicates hard collinear divergences, which have to cancel with the universal contributions coming from hard mass factorization (HMF). The collinear phase space region, which appears for all $2 \rightarrow 3$ kinematics, is defined as the region in which the value of the corresponding invariant for the two possibly collinear momenta p_i and p_j falls below $(p_i + p_j)^2 < \delta_c s$, where \sqrt{s} is the partonic center of mass energy. The non-collinear phase space region is finite and can be integrated over numerically, creating an implicit logarithmic dependence on the cutoff δ_c . Applying the hard mass factorization corrections, we subtract the

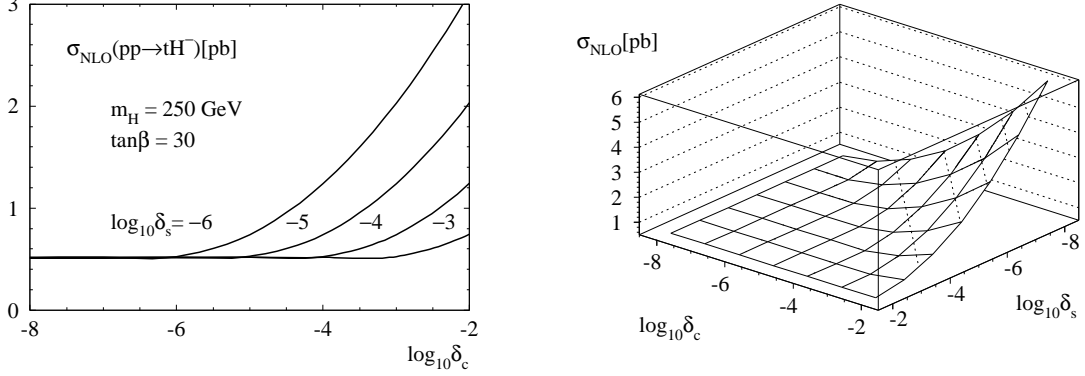


Figure 2: Cross section dependence on the cutoff parameters δ_c and δ_s at the LHC energy. Left: The soft cutoff δ_s is fixed to different values. Right: two dimensional logarithmic dependence on both cutoff parameters.

hard-collinear contributions as a convolution of the leading order matrix element and the appropriate finite splitting function, multiplied by $\log \delta_c$ [22]. The mismatch of pre-factors leads to an additional explicit dependence of the NLO cross section on the factorization scale $\log \mu_F$.

The situation for the virtual and real gluon emission in the gb initial state is slightly more involved, because additional divergences appear due to soft gluon emission. Soft gluon emission is defined by the non-invariant gluon energy constraint $E_g < \delta_s \sqrt{s}/2$. The cross section can be written as

$$d\sigma_g = d\sigma_{\text{virt}}^S + d\sigma_{\text{virt}}^{\text{SC}} + d\sigma_{2 \rightarrow 3}^S + d\sigma_{2 \rightarrow 3}^{\text{SC}} + d\sigma^{\text{SMF}} + d\sigma_{2 \rightarrow 3, g}^{\text{HC}} + d\sigma_{2 \rightarrow 3, g}^{\text{finite}} + d\sigma_g^{\text{HMF}}. \quad (6)$$

The additional soft $1/\epsilon$ and overlapping soft-collinear $1/\epsilon^2$ divergences appear in the virtual as well as in the real gluon emission, they are universal and cancel with soft contributions from mass factorization. Again, we integrate numerically over the hard and non-collinear part of phase space and obtain an implicit dependence on $\log \delta_s$ and $\log \delta_c$.

After the purely soft divergences are canceled between the different $d\sigma^S$ and $d\sigma^{\text{SC}}$ contributions, and the pre-factors between real and the virtual gluon emission diagrams are matched, no explicit scale dependence occurs in dimensional regularization. After the soft divergences are removed, all poles in $d\sigma^S$ and all double poles in $d\sigma^{\text{SC}}$ vanish, and only single collinear poles $1/\epsilon$ remain in $d\sigma^{\text{SC}}$. Cancellation of these remaining divergences with the soft mass factorization contribution (SMC) renders a finite virtual gluon emission matrix element with an additional explicit dependence on $\log \delta_s$, which will cancel with the implicit dependence of the numerically integrated hard non-collinear phase space. It also introduces an explicit dependence on the factorization scale $\log \mu_F$ in the universal mass factorization terms (SMF). Last, as a slight complication, the same soft-collinear phase space configurations, which include an explicit $\log \delta_c$ factor, also lead to an implicit $\log \delta_s$ dependence after the numerical phase space integration. This dependence again cancels with the cutoff dependence of the $2 \rightarrow 3$ phase space, but makes the numerical analysis tedious [22].

Both cutoff parameters, δ_s and δ_c , must be small in order for the soft and collinear approximation of the universal terms to be valid. Physical observables should not depend on the cutoff parameters appreciably. We have checked in detail that for sufficiently small values of δ_s and δ_c the NLO cross section and the distributions approach a two dimensional plateau. To define the soft and the collinear regions of phase space consistently and to avoid double counting, it is most convenient to require $\delta_c \ll \delta_s$ and then determine the one dimensional plateau for a fixed relation between δ_s and δ_c . We show the behavior of the cross section versus the soft and the collinear cutoffs in Fig. 2 at the LHC energy. Indeed the cross section develops a wide plateau for $\delta_c \lesssim \delta_s$. Checking the two dimensional plateau and comparing it with results for the total cross section obtained with a one cutoff method [14], we find that our NLO cross section has a remaining uncertainty of 0.1% – 0.5% due to the cutoff dependence and the corresponding numerical uncertainty.

B. Scale Dependence

Perturbative QCD calculations introduce an unwelcome dependence in the prediction of observables on the renormalization scale μ_R and the factorization scale μ_F . One of the major motivations to perform NLO calculations is to reduce this scale dependent theoretical uncertainty in predictions of the physical observables. As the default renormalization scale, we choose Eq. (2), related to the hard scale M . We identify the renormalization scales of the strong coupling and the Yukawa coupling. It has been demonstrated that this central renormalization scale choice leads to perturbatively stable predictions for cross sections

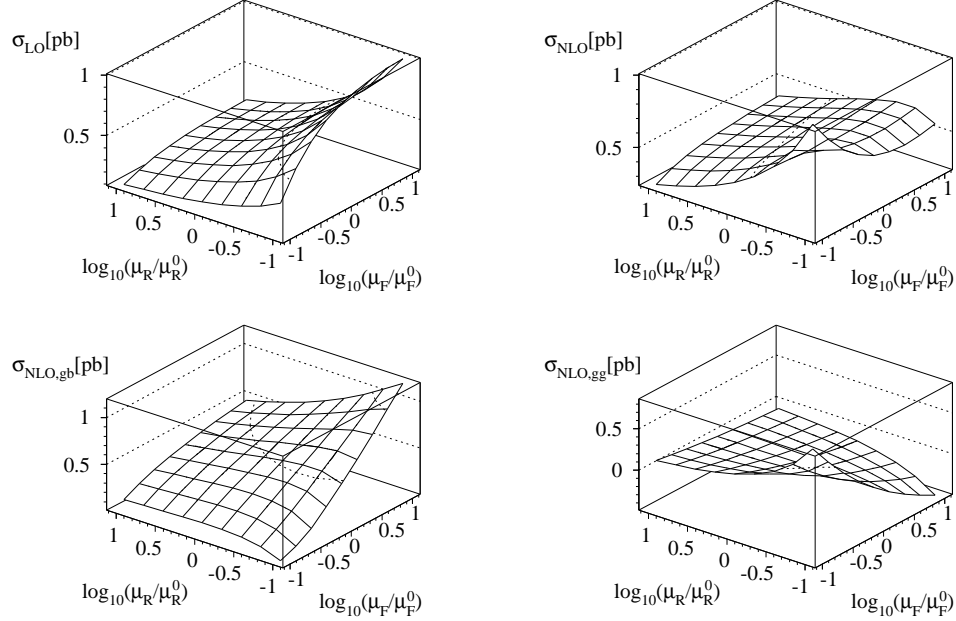


Figure 3: The scale variation of the cross sections at the LHC for $m_H = 250$ GeV and $\tan \beta = 30$. The central values are $\mu_R^0 = M/2$ and $\mu_F^0 = M/5$. The four panels show the leading order cross section, the complete NLO cross section, the gb induced NLO cross section and the gg induced contribution to the NLO cross section.

and branching fractions as functions of α_s [25, 29] as well as functions of y_b [30]. The situation is different for the factorization scale. Two reasons point to a central scale considerably smaller than the hard scale M , an optimum choice being $\mu_F = M/5$:

First, we can estimate the factorization scale from the kinematics of the exclusive process $gg \rightarrow \bar{b}tH^-$. The bottom quark factorization scale may be defined as the maximum $p_{T,b}$ which is included in the inclusive process, the transverse momentum ‘size’ of the parton; for the perturbatively calculated bottom quark density we can go back to the exclusive process $gg \rightarrow \bar{b}tH^-$ and estimate up to which value $p_{T,b}^{\max}$ the cross section shows the asymptotic behavior $\sigma_{\bar{b}tH^-} \sim 1/p_{T,b}$. We find that the hadronic phase space or more specifically the gluon luminosity cuts off the asymptotic behavior around $p_{T,b}^{\max} \sim M/5$, and we can understand this behavior independently from the form of the matrix element, as long as both incoming partons are either gluons or bottom quarks [14, 15]. A remaining problem might be that from basic principles it is not clear if one could use the (factorizing) internal momentum transfer Q_b instead of $p_{T,b}$ [16]. The difference in the maximum value up to which the asymptotic form holds is $p_{T,b}^{\max} \sim Q_b^{\max}/2$, and the plateau in $p_{T,b}$ is considerably softened [15]. We take this uncertainty into account by varying the factorization scale over a generous range. Note that our argument works because the bottom parton density is perturbatively calculated, which means that its features are well defined and perturbatively understood.

Second, in the similar process $b\bar{b} \rightarrow h$ the explicit NNLO corrections are indeed perturbatively most stable for, and therefore point to, the same small factorization scale [18]. Moreover, the NLO corrections to the similar process $b\bar{b} \rightarrow W^+H^-$ are negative for $\mu_F = M$ [9], indicating possibly much too large a collinear subtraction.

The variation of the total cross section with the factorization and renormalization scales is discussed in Ref. [14]. The cross section is under control perturbatively if the two scales μ_R and μ_F are varied independently. However, there is a very large shift in the total rate if the two scales are varied together $\mu_R \propto \mu_F$ and run to very small values $\mu \lesssim M/10$. This behavior suggests the presence of large contributions $\log \mu_R \times \log \mu_F$, which we investigate in more detail. In Fig. 3 we show the scale dependence of the different contributions to the leading and next-to-leading order cross section for the inclusive production process $gb \rightarrow tH^-$. The leading order curve (upper-left) behaves as one would expect, namely the cross section increases for small μ_R and for large μ_F independently of each other. This behavior arises from the running strong coupling α_s and the bottom parton distribution. The running bottom Yukawa coupling in contrast is relatively constant for these large scales. The gb initiated NLO curve (lower-left) is also easy to understand. The cross section increases with the (bottom quark) factorization scale, but it develops a maximum value as a function of μ_R at a physical value of the scale, for not values of μ_F not too large. The fraction $\sigma_{\text{NLO},gb}/\sigma_{\text{LO}}$ is perturbatively under control over the range of scales, varying at most 20% (see a later discussion). The corrections are largest (and negative) for small μ_R , because α_s is largest there. We note that use of the bottom quark pole mass as the Yukawa coupling gives an unacceptably large leading order cross section and leads to perturbatively unstable rates. The

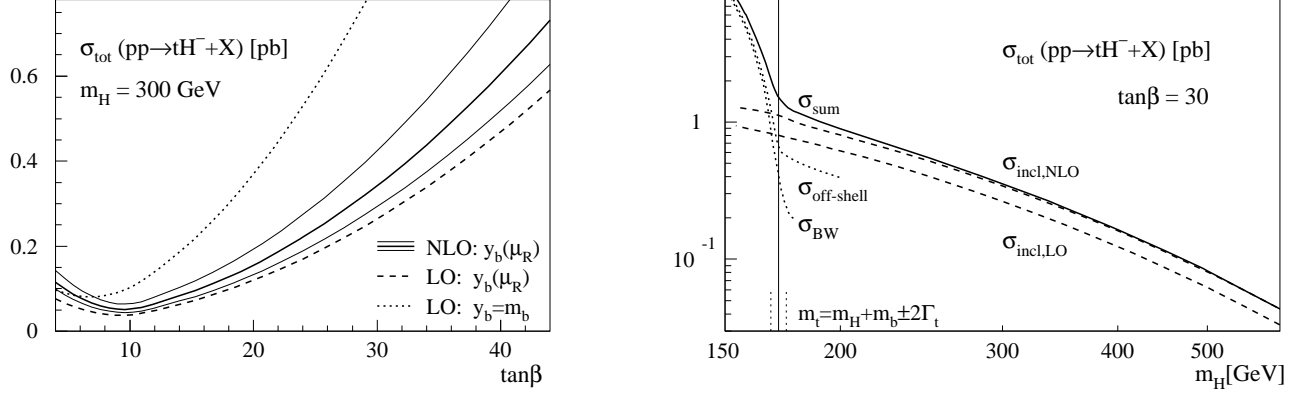


Figure 4: Left: The inclusive $gb \rightarrow tH^-$ cross section at the LHC as a function of $\tan\beta$. The solid curve is the NLO result, with the scale variations around the central scale $\mu/\mu_0 = 1/4 - 4$ indicated by the thinner solid curves. Also shown are the leading order result with a running bottom quark Yukawa coupling (dashed curve) as well as a pole mass Yukawa coupling (dotted curve). Right: The total cross section at the LHC as a function of the charged Higgs boson mass as the solid curve. The NLO and LO cross sections are shown as the dashed upper and lower curves, respectively. The dotted curves show the cross sections for $pp \rightarrow t\bar{t}^* + X$ with a subsequent decay $\bar{t} \rightarrow \bar{b}H^-$ in the Breit-Wigner approximation (σ_{BW}) and that including the complete set of off-shell diagrams ($\sigma_{\text{off-shell}}$).

$gg \rightarrow \bar{b}tH^-$ contribution (lower-right) to the NLO rate has a very different behavior, which dominates the complete NLO rate. The gg contribution is regularized through mass factorization, which means that we compute the exclusive process subtracting out the contribution which is included in the collinear bottom quark splitting. For a central $\mu_R \sim \mu_R^0$ we indeed see that the gg channel gives a small positive contribution for small μ_F and a small negative contribution for large μ_F . The latter indicates that the large scale choice overestimates the logarithms, which is then corrected for by the explicit NLO diagram. If we do not take into account the difference in size of gluon and bottom parton luminosities, the gg initialized process is suppressed by a factor α_s as compared to the inclusive gb process. If we decrease μ_R and thereby increase α_s the correcting behavior pattern stays, but it becomes much steeper. For a central value $\mu_F \sim \mu_F^0$ the gg initial state corrections are zero, and for much larger or smaller μ_F their absolute value increases sharply. The gg contribution blows up for small μ_F and simultaneously small μ_R . We can understand this effect if we take the position that the choice of very small μ_F and very small μ_R corresponds to a region in parameter space where the gb initial state is not perturbatively dominant. This result arises because we choose to ignore the presence of large collinear logarithms up to $p_{T,b}^{\text{max}} \equiv \mu_{F,b}$ and at the same time we push α_s to large values. As expected the K factor blows up, indicating that we should use the exclusive process $gg \rightarrow \bar{b}tH^-$ as the leading process.

C. Total cross section at the LHC

The effects of the NLO corrections on the total cross sections for the inclusive process $gb \rightarrow tH^-$ at the LHC are shown in Fig. 4, versus $\tan\beta$ and versus the charged Higgs boson mass m_H . The solid curve shows the NLO cross section, with the scale variations around the central scale $\mu/\mu_0 = 1/4 - 4$ indicated by the thin solid lines in the left panel. The total cross section increases for large values of $\tan\beta$, as expected for the leading behavior $\sigma_{\text{tot}} \propto \tan^2\beta$, while the K factor is fairly independent of $\tan\beta$ [14]. At leading order we compare the cross section predictions for running bottom quark Yukawa coupling and the pole-mass Yukawa coupling. As expected, the pole-mass Yukawa coupling overestimates the total production rate, while the leading order rate with a running bottom quark Yukawa coupling is perturbatively stable. With the running bottom quark Yukawa coupling, the NLO result is slightly enhanced by a factor of $K \sim 1.4$ [14]. The scale variation suggests a remaining theoretical uncertainty of about 20% on the NLO cross section prediction. Both results confirm that the perturbative behavior of the production process $gb \rightarrow tH^-$ is under control.

In the right panel of Fig. 4, the NLO and LO cross sections are given by the dashed upper and lower curves, respectively. The size of the NLO corrections is essentially independent of the Higgs boson mass, a uniform enhancement factor of about 1.4. The process $gb \rightarrow tH^-$ itself is well defined over the entire Higgs boson mass range, as long as the hard scale $M = m_H + m_t$ is sufficiently large to motivate the bottom parton picture.

An interesting region is one in which the still sizable Higgs boson mass becomes of the order of the top quark mass or smaller and the decay $t \rightarrow bH^-$ is possible. In Fig. 4 we see that the production of a top quark pair $pp \rightarrow t\bar{t} + X$ with a subsequent (off-shell) decay $\bar{t} \rightarrow \bar{b}H^-$ becomes the dominant process. This result is not surprising, since for $m_H \lesssim m_t$ the production cross section is of the order α_s^2 instead of $\alpha_s y_{b,t}^2$, and it probes the large gluon luminosity at the LHC in this partonic energy range. In the following we discuss how these two processes can be combined, to obtain the best cross section prediction over the

entire Higgs boson mass range.

For small Higgs boson masses, below the threshold $\bar{t} \rightarrow \bar{b}H^-$, the $t\bar{t}$ production process with a subsequent decay of the anti-top will dominate the rate for associated charged Higgs boson production. It is straightforward to combine the $t\bar{t}$ production process with subsequent decay $\bar{t} \rightarrow \bar{b}H^-$, and the *exclusive* production channel $pp \rightarrow \bar{b}tH^- + X$ with a tagged final state bottom-quark jet [26]. We compute the process $pp \rightarrow \bar{b}tH^- + X$ with a finite top-quark width, essentially giving us a Breit–Wigner propagator for the intermediate anti-top quark. Gauge invariance can be achieved in the overall factor scheme [24], in which additional terms $\mathcal{O}(\Gamma_t/m_t)$ are traded for a gauge invariant matrix element. In Fig. 4 (the dotted curves in the right panel) we see that the exclusive process $\bar{t} \rightarrow \bar{b}H^-$ is approximated well by the subset of diagrams with an intermediate anti-top in the Breit–Wigner approximation, as long as the Higgs boson mass stays below the top quark threshold. Above the top quark threshold, the exclusive process $pp \rightarrow \bar{b}tH^- + X$ is dominated by the continuum off-shell diagrams, *i.e.* the off-shell extension of the $t\bar{t}$ production process, including all the diagrams initiated from $q\bar{q}$ and gg . In Fig. 4 these off-shell diagrams become dominant where the cross section flattens and settles below the inclusive rate, while the Breit–Wigner cross section becomes very small.

For Higgs boson masses above threshold, tagging the bottom jet is a heavy price to pay and likely it is a better idea to consider the bottom–inclusive process. Then the collinear logarithms become large and for the best possible prediction of the rate we must consider the inclusive process $gb \rightarrow tH^-$ [14], keeping in mind that even at threshold the hard scale of the process is $M = 350 \text{ GeV} \gg m_b$. The difference between the inclusive bottom–gluon induced rate and the off-shell curve in Fig. 4 shows this enhancement of the inclusive rate due to the resummed logarithms. Strictly speaking we have to take into account that off-shell production also includes the quark–initiated channels $q\bar{q} \rightarrow \bar{b}tH^-$, which do not contribute to the bottom parton density at leading order, but they contribute only about 10% to the total exclusive rate. The matching of the small and large Higgs boson mass regimes in Fig. 4 indicates that we need a combination of the $t\bar{t}$ production process with the bottom–inclusive process $gb \rightarrow tH^-$. There appears to be no region of Higgs boson masses where the off-shell production process $gg \rightarrow \bar{b}tH^-$ is the appropriate perturbative description. Note that in Fig. 4 we show the different $t\bar{t}$ cross sections with a finite bottom quark mass, while we neglect the bottom quark mass for the inclusive channel. The uncertainty induced by this approximation is small, however, since we cannot avoid neglecting Γ_t/m_t corrections and $m_b/M \sim \Gamma_t/M$.

At leading order there is no problem in combining the Breit–Wigner approximation of the $pp \rightarrow t\bar{t}^* + X$ process with a subsequent decay of the anti-top and the inclusive process $gb \rightarrow tH^-$. We can just add the independent event samples for any Higgs boson mass value. However, at NLO and for Higgs boson masses smaller than the top quark mass there occurs a potential problem of double counting. The $t\bar{t}^*$ production process with a subsequent decay of the (off-shell) anti-top can be regarded as an $\mathcal{O}(\alpha_s)$ correction to the gb initiated inclusive process, Eq. (4), while it can as well be viewed as (nearly) on-shell $t\bar{t}$ production with a subsequent decay $\bar{t} \rightarrow \bar{b}H^-$. To avoid this double counting, we subtract the resonant on-shell parts of the $t\bar{t}$ diagrams from the NLO correction to the inclusive process and keep it as part of the $pp \rightarrow t\bar{t} + X$ rate [25]. The non-divergent off-shell contribution of the \bar{t}^* propagator is counted toward the NLO inclusive rate. The division into on-shell and off-shell contributions, however, is well defined only in the narrow width approximation, so we will neglect terms of the order Γ_t/m_t . The ambiguity reflects the unsolved problem of how to treat a long lived intermediate particle in field theory. Up to finite width corrections we can, just as at leading order, add the rate for $t\bar{t}$ production with a Breit–Wigner propagator and the properly subtracted NLO $gb \rightarrow tH^-$ rate to obtain a valid cross section prediction for any given Higgs boson mass. In Fig. 4 we see that addition of the cross sections is essentially equivalent to a naive matching procedure. It is perhaps unexpected that the corrections from the Breit–Wigner propagator extend to large Higgs boson masses. On the other hand, keeping in mind that the remaining theoretical uncertainty on the NLO cross section for the gb induced inclusive process is about 20% [14], we see that the details of this matching/adding procedure are phenomenologically irrelevant. Instead of including the on-shell production with the Breit–Wigner propagator for Higgs boson mass values above 300 GeV we could as well have cut it off at $m_H = m_t + 10\Gamma_t$ or whatever number we would choose to pick.

How does one best predict the production cross section for a charged Higgs boson in the mass range below and above the $\bar{t} \rightarrow \bar{b}H^-$ threshold? Below threshold the Breit–Wigner description is valid, with higher order contributions included in the cross section for $pp \rightarrow t\bar{t} + X$ [27, 28]. Off-shell effects have little impact there. Above threshold these off-shell effects have a considerable impact relative to the Breit–Wigner description, but the inclusive cross section $gb \rightarrow tH^-$ is dominant. After the on-shell contributions are subtracted from the NLO rate for $gb \rightarrow tH^-$, we can match the two results by simply adding them, without running into any problem with double counting.

D. Production at the Tevatron

The successful matching of the Breit–Wigner approximation and the inclusive process $gb \rightarrow tH^-$ which we observe for the LHC does not apply readily at the Tevatron. In Fig. 5 we observe that the LO inclusive process $gb \rightarrow tH^-$ underestimates the cross section compared to the exclusive $\bar{b}tH^-$ production [26]. On the other hand, we know that at the Tevatron the gluon luminosity is not dominant in the relevant region of partonic x . The gluon initial state contributes only about 10% to the total

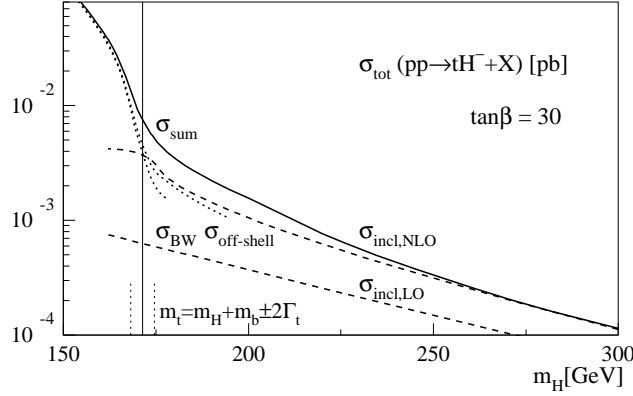


Figure 5: The cross section for the Tevatron (2 TeV) as a function of the charged Higgs boson mass. We also show the cross sections for $pp \rightarrow t\bar{t}^* + X$ with a subsequent decay $\bar{t} \rightarrow \bar{b}H^-$ in the Breit–Wigner approximation and including the complete set of off-shell diagrams.

$pp \rightarrow \bar{b}tH^- + X$ rate. Because initial state gluons are the dominant sources of the bottom partons we expect the leading order inclusive rate to be far smaller than the exclusive rate. The difference between the leading order inclusive rate and the off-shell $\bar{b}tH^-$ production rate is slightly less than a factor 10 because the inclusive rate is still enhanced by the resummation of large logarithms in the bottom parton picture.

The NLO inclusive rate consistently includes the whole set of quark initiated processes, Eq. (4). Because these quark processes are dominant, as compared to the gluon initial state which gives rise to the bottom partons, the K factor for the inclusive process can be as large as 5 for $m_H \sim 175$ GeV. The NLO inclusive rate matches the exclusive off-shell calculation well, particularly considering possible remaining differences between these two channels. The exclusive cross section is evaluated with leading order running couplings and parton densities, while the quark-initiated contributions to the NLO inclusive rates are evaluated with NLO quantities. Moreover, the collinear divergences in the exclusive rate are regularized by a physical bottom quark mass, while the NLO inclusive rate neglects the bottom quark mass and is regularized by mass factorization, *i.e.* subtracting the divergent contributions to avoid any double counting with the NLO evolution of the parton densities.

Just as for the LHC we see that the Breit–Wigner approximation and the complete off-shell matrix element evaluation agree very well up to $m_H \sim m_t$. Above threshold the LO inclusive rate is significantly smaller than the complete off-shell rate, but the NLO inclusive rate matches the exclusive rate well. The visible effect which the Breit–Wigner contribution has on the matched/added sum of the cross sections may be unexpected, but we keep in mind the substantial theoretical uncertainty on the NLO inclusive prediction. The NLO contribution from the exclusive $q\bar{q} \rightarrow \bar{b}tH^-$ production process is larger than the LO gb induced rate. The formally NLO gb induced rate enters with a much wider band of uncertainty than the 20% we quote for the perturbatively well behaved LHC process. This wider band covers different schemes for phasing out the Breit–Wigner contribution toward large Higgs boson masses, where it is not applicable. In Fig. 5 we cut off the Breit–Wigner cross sections for Higgs boson masses between 200 GeV and 250 GeV, *i.e.* roughly 20 top quark widths above threshold.

Although we obtain a predicted cross section at the Tevatron for the entire range of m_H , we emphasize that the matching of the Breit–Wigner production process and the inclusive gb fusion works only if we take into account the NLO corrections to the inclusive channel. At the LHC the same matching of the two approaches at threshold makes sense even for the leading order inclusive $gb \rightarrow tH^-$ rate. Because the bottom parton picture is perturbatively stable at the LHC energy, the prediction of the charged Higgs boson production rate suffers from smaller theoretical uncertainty.

III. KINEMATIC DISTRIBUTIONS AND BOTTOM PARTONS

The underlying concept for the calculation of the production cross section is the bottom parton picture. As reported above, it is evident that the bottom parton description indeed works well and provides an appropriate way to compute total charged Higgs boson production cross sections (if a correct bottom quark factorization scale is used). Extending our analysis from corrections to the total rate to higher order effects on the kinematic distributions we establish three results. First, the normalized distributions of sufficiently inclusive variables for the heavy final states should not change too much when we switch from the LO to the NLO inclusive process $gb \rightarrow tH^-$. Second, the distributions as well as the total rate should not have a strong scale dependence. In particular, checking the limit $\mu_F \rightarrow m_b$, we ensure that the bottom parton picture does not have much impact on the shape of the heavy state kinematic distributions. Finally, we test the approximation of vanishing bottom quark mass in the phase space and the matrix elements, as we employ it in our LO and NLO computations of the inclusive rate.

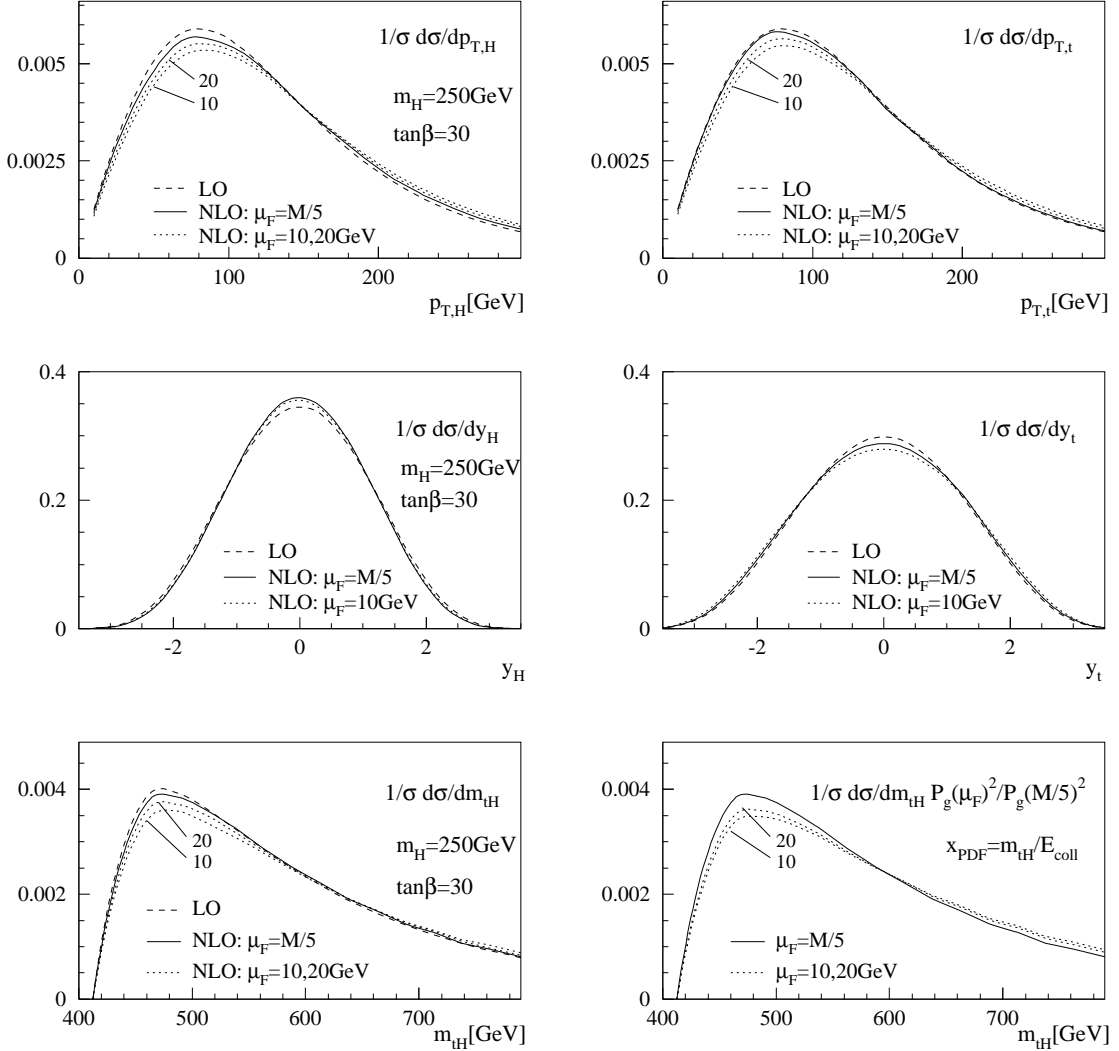


Figure 6: The kinematic distributions for the heavy final state particles at the LHC: transverse momentum and rapidity of the charged Higgs boson (left) and the top quark (right) for the inclusive process $gb \rightarrow tH^-$. The dashed curve shows the leading order distribution with the central choice of scales. The solid and the dotted curves represent the NLO results for three choices of the bottom quark and the gluon factorization scale $\mu_F = M/5$, $\mu_F = 20$ GeV and $\mu_F = 10$ GeV. The bottom row shows the distribution of the invariant mass of the top quark and the Higgs boson pair from the LO and NLO calculations, plus a rescaled NLO distribution (the last panel). The scaling factor involves the gluon parton densities at the different factorization scales.

The first statement is easy to confirm. In Fig. 6 we show the rapidity, transverse momentum and the invariant mass distributions for the heavy final state particles. Even though the additional bottom jet in the final state absorbs part of the momentum from the incoming partons, the NLO transverse momentum distributions become minimally harder. The new, purely quark initiated production process has a considerably harder p_T spectrum but contributes only 10% to the NLO rate (see also the quark induced contribution in the left panel of Fig. 7). For single particle spectra, we conclude that at the LHC the shift in the final state distributions from the LO to the NLO inclusive rate is smaller than the typical scale uncertainty of 20% on the NLO rate. Similar behavior has been found, for example, in the production of heavy supersymmetric particles at NLO [25, 31].

A. Zero transverse momentum approximation

The transverse momentum and the rapidity distributions of the heavy final state particles are depicted in Fig. 6. The choice of the bottom quark factorization scale $\mu_F = M/5$ has been shown to be a part of the consistent bottom parton picture for this

class of processes at the LHC [14, 15, 16]. It remains to be checked whether the collinear approximation for the gluon splitting into a bottom parton is appropriate for the distributions of the final state particles.

To test the bottom parton approach and in particular the approximation of negligible transverse momentum of the incoming bottom parton we make use of the method described in Sec. II B. If the bottom quark factorization scale approaches the bottom quark mass $\mu_{F,b} \rightarrow m_b$ the bottom parton density vanishes. For consistency reasons we use the same factorization scale for all partons, but neither the gluon density nor the light quark densities change dramatically as $\mu_F \rightarrow m_b \gg \Lambda_{\text{QCD}}$. In this limit the NLO gb induced cross section at the LHC will be dominated by the process $gg \rightarrow btH^-$. Even though the final state bottom quark is massless in the calculation, the corresponding rate is finite and well defined for any factorization scale $\mu_F > m_b$. All divergences in the exclusive process, which are originally regularized by a bottom quark mass, are now absorbed into the definition of the NLO parton densities. As described in Sec. II B the physics picture when the bottom quark factorization scale takes the limit $\mu_{F,b} \rightarrow m_b$ is the shift from the resummed cross section including a large logarithm $\log p_{T,b}/m_b$ to the exclusive $\bar{b}tH^-$ production cross section, in which the large logarithm could for example be removed by a $p_{T,b}^{\text{min}}$ detector cut. We show the difference between the NLO distributions with the central factorization scale $\mu_F = M/5$ and the small scale limit in Fig. 6. The scales we use are $\mu_F = 10, 20$ GeV; in principle, we could as well go to $\mu_F = 5$ GeV, for which the calculated bottom quark density is well defined, but the parton densities of gluons and light quarks are poorly constrained. Indeed, we checked that we would then see all the features described below for scales down to 10 GeV, except that their effect on the cross sections would be numerically more pronounced.

Looking at Fig. 6, we see that the final state top quark and Higgs boson become somewhat harder when we increase the contributions from the $2 \rightarrow 3$ matrix elements, going to $\mu_F = 20$ GeV and $\mu_F = 10$ GeV. The same behavior is seen in the invariant mass of the top quark and the Higgs boson pair, m_{tH} , again shown in Fig. 6. To explore this feature we present a normalized distribution of the m_{tH} invariant mass, in which we rescale the gluon distribution function for the central scale $\mu_F = M/5$ by a factor $P_g(\mu_F, x_{\text{PDF}})^2 / P_g(M/5, x_{\text{PDF}})^2$, to estimate the effect of the parton densities. Because most of the cross section arises from production near threshold, we can approximate $x_{\text{PDF}} = m_{tH}/E_{\text{coll}}$ with $E_{\text{coll}} = 14$ TeV. The physics motivation of this cross check is that the gluon densities become slightly harder for smaller scales, *i.e.* we want to understand if the hardening of the m_{tH} distribution is due to the shift from the bottom parton picture to the gluon fusion picture or if it is due to an over-all hardening of the gluon parton spectrum. Indeed, in Fig. 6 we observe that scaling the usual NLO distribution with the x dependence of the gluon parton density reproduces the hardening of the top quark and Higgs boson spectrum. Concluding this argument, we find a slight shift in the spectrum when going to smaller factorization scales, but this shift is induced by the shape of the gluon parton density. The quality of the bottom parton approximation can be appreciated from the two sets of distributions in the bottom row of Fig. 6 — there appears to be no problem with the bottom parton approximation for sufficiently inclusive distributions of the heavy final state particles at the LHC. While there is a large logarithm $\log p_{T,b}/m_b$ present in the exclusive $\bar{b}tH^-$ production rate, there appear to be no additional perturbative pitfalls in the inclusive process after this logarithm is resummed. All additional dependence on the (neglected) transverse momentum of the final state bottom jet is effectively power suppressed.

B. Zero bottom quark mass approximation

We have compared the inclusive gb induced process with the exclusive process $gg \rightarrow \bar{b}tH^-$ without a finite bottom quark mass in the phase space or in the matrix element. For the kinematic distributions of the bottom quarks this approximation is not obviously good. In our NLO approach the divergences in the $p_{T,b}$ spectrum will be compensated by a negative infinity at $p_{T,b} = 0$, *i.e.* in the $2 \rightarrow 2$ kinematic limit. This distribution is not physical, and all-orders soft gluon resummation should be taken into account [32] to obtain a physical spectrum with a peak at some small value of $p_{T,b}$. With the bottom quark mass as a regulator, the $p_{T,b}$ spectrum will peak near m_b [14]. However, when we use the inclusive gb process we are explicitly not interested in observing the final bottom-quark jet and in its distributions, rather, we are interested in the distributions of the heavy final state particles. In Fig. 7 we show the normalized transverse momentum distribution of the top quark for the inclusive process at NLO, and for the exclusive process, with two different cutoffs: one with the physical bottom quark mass and the other with a smaller mathematical cutoff (we use $1/10$ of the bottom quark pole mass). We observe that the inclusive calculation agrees with the exclusive matrix element using the physical bottom quark mass. The curve with a smaller cutoff instead of the bottom quark mass agrees perhaps too well with the NLO process in which the bottom quark mass is neglected. The distribution in the invariant mass of the tH^- final state confirms this level of agreement. We conclude that the dependence on the bottom quark mass seems to be power suppressed, and the approximation of zero bottom quark mass is justified.

However, we also see the limitations of our argument for charged Higgs boson production at the Tevatron. The exclusive rate with a finite bottom quark mass, induced by incoming quarks, shows considerably harder final state top quarks. For the Tevatron cross section this might mean that while the total cross section is predicted correctly in the bottom parton picture, the distributions require more careful study. This effect has nothing to do with the zero bottom quark mass approximation. Instead,

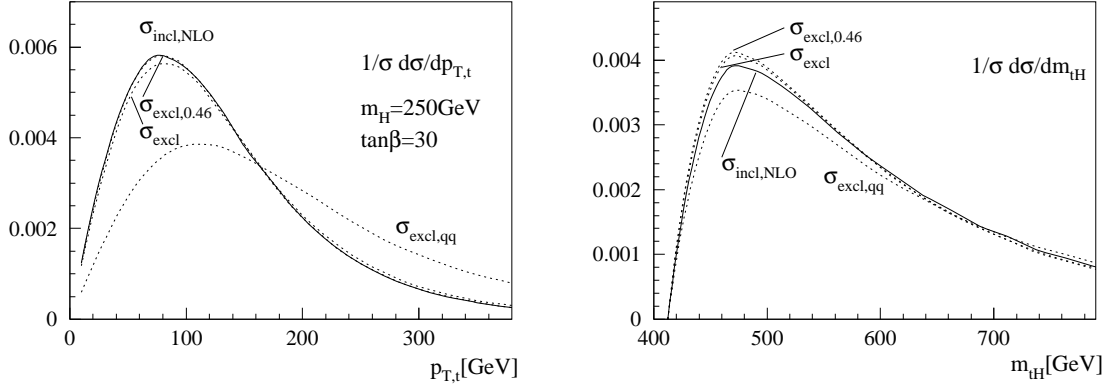


Figure 7: The kinematic distributions for the final state at the LHC: the top quark transverse momentum and the invariant mass of the top quark and the Higgs boson pair. We compare the NLO result for the inclusive process $gb \rightarrow tH^-$ with the exclusive process $pp \rightarrow \bar{b}tH^- + X$. Apart from the complete exclusive set of diagrams with the physical bottom quark mass we show the purely $q\bar{q}$ induced process and the complete set of diagrams with a mathematical cutoff instead of the physical bottom quark mass $m_b \rightarrow 0.46$ GeV.

mSUGRA	m_H	$\tan \beta$	m_0	$m_{1/2}$	A_0	μ	$\sigma_{\text{LO}}[\text{fb}]$	$\sigma_{\text{NLO}}[\text{fb}]$	Δ_b	Δ_b^{resum}	non- Δ_b		
1a	402	10	100	250	-100	352	18.7	25.6	-11.0%	-10.2%	-1.9%		
1b	543	30	200	400	0	501	47.1	61.7	-27.9%	-23.5%	-4.6%		
2	1446	10	1450	300	0	125	0.09	0.13	-0.92%	-0.91%	-1.7%		
3	578	10	90	400	0	509	5.81	8.02	-10.1%	-9.5%	-1.1%		
4	416	50	400	300	0	377	304	395	-39.0%	-31.0%	-4.6%		
5	699	5	150	300	-1000	640	3.73	5.73	-8.5%	-8.0%	0.8%		
mSUGRA-like			m_0	$m_{1/2}$	A_0	M_1	$M_{2,3}$						
6	470	10	150	300	0	480	300	394	11.6	16.0	10.2%	-9.5%	-1.3%
GMSB			Λ	M_{mes}	N_{mes}								
7	387	15	40×10^3	80×10^3	3	300	36.5	48.0	-8.5%	-8.1%	-0.9%		
8	521	15	100×10^3	200×10^3	1	398	15.0	20.4	-7.5%	-7.1%	-0.5%		
AMSB			m_0	m_{aux}									
9	916	10	400	60×10^3		870	0.92	1.29	-10.6%	-9.9%	4.1%		

Table I: Supersymmetric corrections to the production cross section $gb \rightarrow tH^-$ from non-resummed and resummed Δ_b corrections, Eq. (7), and from the explicit remaining supersymmetric loop diagrams. The supersymmetric parameter points are chosen according to the benchmarks in Ref. [36]. All masses are given in units of GeV. The percentage changes are defined with respect to the purely gluonic NLO rates.

it probes the perturbative link between the contribution of gluon and quark initiated diagrams in the exclusive production process and the bottom parton description.

To summarize this section: not only the total cross section but also the inclusive distributions of the final state particles are correctly predicted in the bottom parton picture. Neither the small transverse momentum approximation nor the small bottom quark mass approximation in the bottom parton picture has a visible effect on the transverse momentum, rapidity, and the invariant mass distribution of the final state top quark and Higgs boson. Tiny shifts induced by the massless bottom parton approximation will be washed out once detector resolution is taken into account. For the processes under consideration, the contribution from the $q\bar{q}$ initial states is less important at the LHC than it is at the Tevatron. If this were not true, these conclusions might change. The light-quark induced subprocesses show considerably harder transverse momentum spectra, which should be considered for predictions at the Tevatron.

IV. SUPERSYMMETRIC CONTRIBUTIONS

At the same level of the NLO QCD contributions ($\alpha_s^2 y_{b,t}^2$), explicit supersymmetric diagrams contribute to the production rate for $gb \rightarrow tH^-$. These diagrams are essentially the virtual gluon exchange diagrams, where the gluons and quarks are replaced

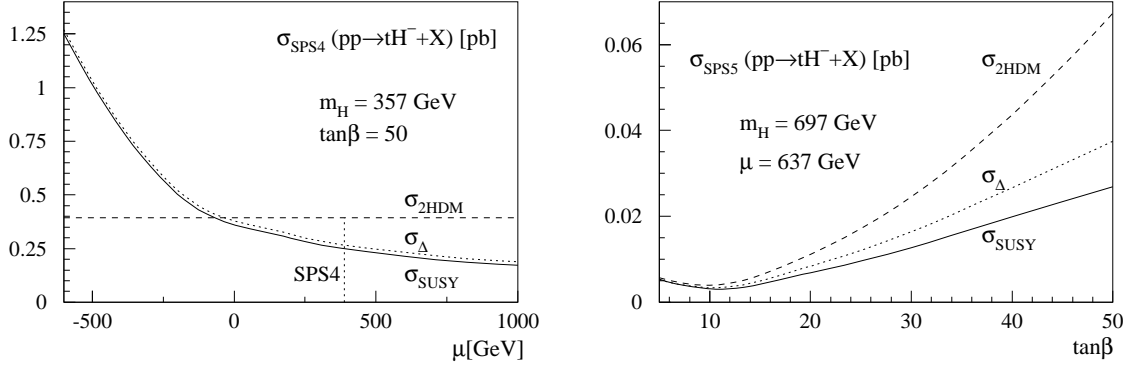


Figure 8: The supersymmetric contributions to the NLO prediction for the inclusive cross section $gb \rightarrow tH^-$, with the dotted curve showing the resummed Δ_b contribution and the solid curve showing the combination of the resummed Δ_b and the non- Δ_b contributions. The supersymmetric parameters are described in Table I. The central μ value in SPS4 is given in the plot; the central $\tan \beta$ value in SPS5 is at the lower end of the plot, $\tan \beta = 5$. All parameters and masses except for μ and $\tan \beta$ are kept constant.

by the supersymmetric partners, gluinos and squarks. A feature of squarks is the mixing between the partners of the left-handed and the right-handed quarks. The 2×2 bottom-squark mass matrix includes an off-diagonal contribution $m_b(A_b - \mu \tan \beta)$, and the top-squark mass matrix has an entry $m_t(A_t - \mu / \tan \beta)$. Here μ is the Higgsino mass parameter which links the two Higgs doublets in the Lagrangian, and A_i is the trilinear squark-squark-Higgs coupling parameter. In general the off-diagonal matrix element entry is proportional to the standard model partner mass, which means that it is usually neglected for the first and second generations. In most models the mixing renders the lighter top squark the lightest strongly interacting sparticle, a particularly promising candidate for hadron collider searches for supersymmetric partners. For large values of $\tan \beta$ the bottom squark mixing can become even larger than the top squark mixing.

In the limit of large $\tan \beta$, the leading supersymmetric contributions are not loop diagrams, but renormalization terms [33]. This point becomes evident if when we compute the corrections to the btH^- vertex in the limit of vanishing bottom quark mass, but finite bottom quark Yukawa coupling. From a formal point of view this approach is justified, because the connection between the mass and the Yukawa coupling is a property of electroweak symmetry breaking and not protected once the symmetry is broken. In a type-II two-Higgs-doublet model like the MSSM the disassociation of the mass and the Yukawa coupling becomes apparent. Because the bottom quark Yukawa coupling always appears as $m_b \tan \beta$, the relation between mass and Yukawa coupling is not fixed. If we compute the renormalization of the tbH^- vertex with a zero external bottom quark mass, bottom squark mixing diagrams lead to contributions which look like mass renormalization terms, *i.e.* terms which create a finite bottom quark mass in the external leg. However, this cannot be correct, since mass renormalization has to be multiplicative. Instead, we see that these renormalization factors describe a misalignment of the bottom quark Yukawa coupling and the bottom quark mass, which appears for zero as well as a finite bottom quark mass. In complete analogy to a mass renormalization these coupling renormalization diagrams can be resummed to all orders and then lead to a correction [35]:

$$\begin{aligned}
 \frac{m_b \tan \beta}{v} &\rightarrow \frac{m_b \tan \beta}{v} \frac{1}{1 + \Delta_b} \\
 \Delta_b &= \frac{\sin(2\theta_b)}{m_b} \frac{\alpha_s}{4\pi} C_F m_{\tilde{g}} \frac{1}{i\pi^2} \left[B(0, m_{\tilde{b},2}, m_{\tilde{g}}) - B(0, m_{\tilde{b},1}, m_{\tilde{g}}) \right] \\
 &= \frac{\alpha_s}{2\pi} C_F m_{\tilde{g}} (-A_b + \mu \tan \beta) I(m_{\tilde{b},1}, m_{\tilde{b},2}, m_{\tilde{g}}) \\
 I(a, b, c) &= -\frac{1}{(a^2 - b^2)(b^2 - c^2)(c^2 - a^2)} \left[a^2 b^2 \log \frac{a^2}{b^2} + b^2 c^2 \log \frac{b^2}{c^2} + c^2 a^2 \log \frac{c^2}{a^2} \right]. \quad (7)
 \end{aligned}$$

The function $B(p^2, m_1, m_2)$ is the usual scalar two-point function; $C_F = 4/3$ is the Casimir factor in the fundamental representation of $SU(3)$. There are similar additional terms proportional to the strong coupling or to the top quark Yukawa coupling, but Eq. (7) is the leading contribution for large $\tan \beta$.

Since these Δ_b corrections are the leading $\tan \beta$ enhanced supersymmetric contributions to the production cross section, and the charged Higgs boson search is most promising at $\tan \beta \gtrsim 15$, we might speculate that these corrections to the $gb \rightarrow tH^-$ production rate will be sufficient. Equation (7) shows that the shift in the Yukawa coupling can have large effects [34]. All we need is large (preferably negative) $\mu \tan \beta$, a large gluino mass, and bottom-squark masses not too large. In this limit the

corrections in percent are approximately $\Delta_b \sim \mu \tan \beta / m_{\tilde{g}}$. On the other hand we show that the non- Δ_b -type supersymmetric corrections are indeed negligible, for example, compared to the remaining NLO scale variation. Expanding an earlier survey [14] we estimate the size of Δ_b -type and non- Δ_b corrections over a wide range of supersymmetric parameters [36].

In Table I we give the supersymmetric contributions to the charged Higgs boson production cross sections for the ‘Snowmass points and slopes’ (SPS). The contributions are split into the Δ_b corrections, as defined in Eq. (7), and the remaining explicit supersymmetric diagrams. We present the Δ_b contributions in the consistent NLO version $1 - 2\Delta_b$ as well as after resummation $1/(1 + \Delta_b)^2$. The ratios of the SUSY corrections to the NLO QCD cross sections are given in the last three columns. The negative sign of the Δ_b contributions is fixed by the sign of μ . The sign of μ is a free parameter, linked to SUSY contributions to the transition rate $b \rightarrow s\gamma$. In this process the measured rate is consistent with the standard model prediction. In the MSSM there are additional charged Higgs boson and chargino induced contributions. For $\mu > 0$ they enter with opposite signs and therefore tend to cancel numerically, while for $\mu < 0$, in particular in the mSUGRA supersymmetry breaking scheme, the parameter space is closely constrained. Therefore, all SPS points are chosen with positive sign of μ .

In Table I we observe that for all points with $\tan \beta \geq 15$ the Δ_b corrections are dominant, particularly for the two points with $\tan \beta = 30, 50$. The leading contribution for large $\tan \beta$ is indeed correctly described by the Δ_b corrections. We also observe that all supersymmetric corrections are at maximum of the order of the remaining scale variation and our estimate of the theoretical uncertainty of 20%, as long as $\tan \beta \lesssim 30$. This modest correction is not necessarily the case for the entire supersymmetric parameter space, and the Δ_b corrections can be much larger [34]. However, it reflects the ansatz used in supersymmetry breaking. None of the scenarios in Table I is designed to produce a large splitting in the supersymmetric mass parameters at the weak scale or a large value of $|\mu|$, which favor large Δ_b -type corrections. In general, large values of $|\mu|$ are a challenge in high-scale motivated models. For fine-tuning reasons these models usually produce $|\mu| \sim m_Z$, to avoid large cancellations of different renormalization group contributions to the value of m_Z . Even in the focus-point [37] inspired SPS2 the contribution to weak-scale parameters that are proportional to m_0 cancels in itself, decoupling the value of m_0 from the leading renormalization group running. All other parameters remain at typical weak-scale values. The large gluino mass, linked in all three SUSY breaking scenario considered to the relative dominance of the corresponding beta function β_3 , is the reason the Δ_b correction is not negligible.

In Fig. 8 we show that the Δ_b contributions can become large once we leave the unification scenarios. Starting from the mSUGRA motivated points SPS4 and SPS5, listed in Table I, we vary μ and $\tan \beta$, leaving all other masses and parameters invariant. As expected, the non-resummed Δ_b corrections become arbitrarily large for large values of $|\mu|$, and the resummed Δ_b correction can become arbitrarily large for some negative μ , both limited only perturbatively and ultimately by unitarity of the enhanced bottom quark Yukawa coupling. The sign of the Δ_b correction is fixed by the sign of μ , and the remaining SUSY contributions are small. In Fig. 9 we show the same effect, starting from the scenarios A and C in Ref. [34]. Because the value of $\tan \beta = 50$ is large, the non- Δ_b corrections are completely negligible, while the Δ_b corrections can become arbitrarily large. The difference in the size of the corrections seen in the two panels of Fig. 9 can be understood from Eq. (7) in the limit $a \sim b$ for the bottom squark masses and either $c \gg a, b$ or $c \sim a, b$. In both cases the Δ_b corrections are suppressed by the heaviest mass in the system, *i.e.* the gluino mass, but the pre-factor is larger if all masses involved are of the same order.

V. CONCLUSIONS

We evaluate the inclusive and differential cross sections for the associated production of a top quark along with a charged Higgs boson at the Tevatron and the LHC energies to next-to-leading order in QCD and in supersymmetric QCD. The main conclusions are:

- * Using the two-cutoff scheme to treat the soft and collinear singularities, we find stable results for total and differential cross sections over large ranges of the cutoff parameters as well as of the factorization and renormalization scales. While the QCD corrections to the total rate are sizable at the LHC, $K \sim 1.4$ [14], the shifts in the normalized kinematic distributions of the heavy final state top quark and Higgs boson are negligible. The scale dependence gives us a reasonable estimate on the remaining theoretical uncertainty of about 20%.
- * We compute the NLO cross section in the regime where $m_H < m_t$, subtracting the intermediate on-shell divergences in the narrow width approximation. This procedure allows us to match the NLO cross section for the process $gb \rightarrow tH^-$ with the contributions from $gg \rightarrow t\bar{t}^*$ with a subsequent decay $\bar{t} \rightarrow \bar{b}H^-$, simply by adding the rates. Along with predictions of the cross section for $t\bar{t}$ production, this method gives a reliable cross section prediction for associated charged Higgs boson production over the entire Higgs boson mass range.
- * At the Tevatron, charged Higgs boson production is likely to be observed only for small Higgs boson masses. In this regime we show that the Breit–Wigner approximation in the $t\bar{t}$ production process is valid, and we can consistently add the off-shell production rate at NLO.

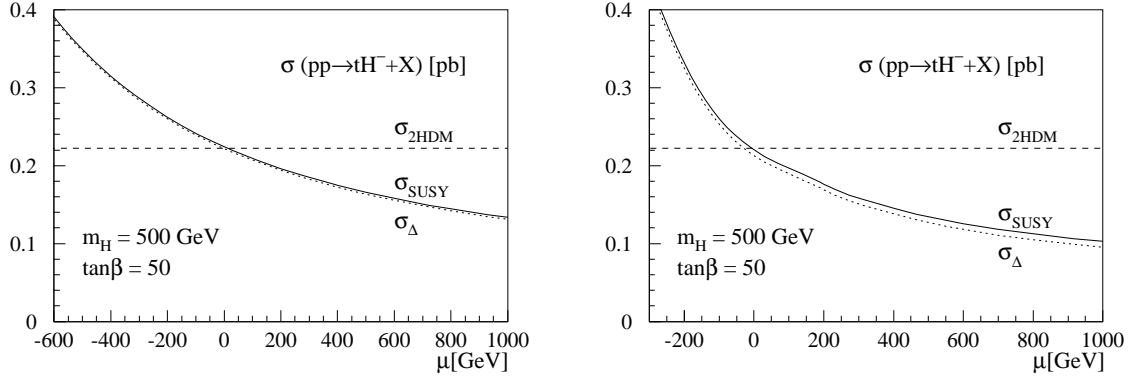


Figure 9: The supersymmetric contributions to the NLO prediction for the inclusive cross section $gb \rightarrow tH^-$, with the dotted curve showing the resummed Δ_b contribution and the solid curve showing the combination of the resummed Δ_b and the non- Δ_b contributions. The supersymmetric parameter points are the scenarios A and C, picked from Ref. [34]. All parameters and masses except for μ are kept constant. The gluino mass in both scenarios is 1 TeV; the lighter top-squark and bottom-squark masses are 0.5 TeV for scenario A (LHS) and 1 TeV for scenario C (RHS). The top-squark mass difference is 100 GeV and the bottom-squark mass difference 150 GeV. In contrast to Ref. [34] we resum only the SUSY-QCD corrections.

- * Comparing NLO distributions for the inclusive charged Higgs boson production process, we show the validity of the bottom parton description beyond the total rate. Neither the collinear phase space approximation nor the zero bottom quark mass approximation has a visible impact on the kinematic distributions of the heavy final state particles.
- * We explore the effects of virtual supersymmetric particles in NLO loop diagrams and find that the universal Δ_b corrections to the Yukawa coupling can be sizable. The remaining explicit loop contributions to the NLO rate are well below the scale uncertainty in the two Higgs doublet model.

Acknowledgments

We thank Brian Harris for his help regarding the two-cutoff method and Shouhua Zhu for providing comparisons between our results and those in Ref. [19]. J.J. acknowledges helpful discussions with John Campbell and Jungil Lee. T.P. wants to thank Sasha Nikitenko for his support and for pointing out questions from the experimental community. Moreover, T.P. wishes to thank Thomas Teubner and Sakis Dedes for helpful discussions, and last but not least the IPPP in Durham for their kind hospitality during the final stage of this paper. The research of E. L. B. and J. J. in the High Energy Physics Division at Argonne National Laboratory is supported by the U. S. Department of Energy, Division of High Energy Physics, under Contract W-31-109-ENG-38. T.H. is supported in part by the DOE under grant DE-FG02-95ER40896, and in part by the Wisconsin Alumni Research Foundation.

-
- [1] D. Abbaneo *et al.* [LEPEWWG], arXiv:hep-ex/0212036.
 - [2] CMS Collaboration, Technical Proposal, CERN/LHCC/94-38 (1994); ATLAS Collaboration, Technical Proposal, CERN/LHCC/94-43 (1994).
 - [3] T. Plehn, D. Rainwater and D. Zeppenfeld, Phys. Lett. B **454**, 297 (1999).
 - [4] U. Baur, T. Plehn and D. Rainwater, arXiv:hep-ph/0310056.
 - [5] F. Abe *et al.* (CDF Collaboration), Phys. Rev. Lett. **79**, 357 (1997); B. Abbott *et al.* (D0 Collaboration), Phys. Rev. Lett. **82**, 4975 (1999).
 - [6] E. Eichten, I. Hinchliffe, K. D. Lane and C. Quigg, Rev. Mod. Phys. **56**, 579 (1984) [Addendum-ibid. **58**, 1065 (1986)]; N. G. Deshpande, X. Tata and D. A. Dicus, Phys. Rev. D **29**, 1527 (1984).
 - [7] J. F. Gunion, H. E. Haber, F. E. Paige, W. K. Tung and S. S. Willenbrock, Nucl. Phys. B **294**, 621 (1987); A. Krause, T. Plehn, M. Spira and P. M. Zerwas, Nucl. Phys. B **519**, 85 (1998); A. A. Barrientos Bendezu and B. A. Kniehl, Nucl. Phys. B **568**, 305 (2000); O. Brein and W. Hollik, Eur. Phys. J. C **13**, 175 (2000).
 - [8] D. A. Dicus, J. L. Hewett, C. Kao and T. G. Rizzo, Phys. Rev. D **40**, 787 (1989); A. A. Barrientos Bendezu and B. A. Kniehl, Phys. Rev. D **59**, 015009 (1999); and Phys. Rev. D **63**, 015009 (2001); O. Brein, W. Hollik and S. Kanemura, Phys. Rev. D **63**, 095001 (2001).
 - [9] W. Hollik and S. H. Zhu, Phys. Rev. D **65**, 075015 (2002).

- [10] R. M. Barnett, H. E. Haber and D. E. Soper, Nucl. Phys. B **306**, 697 (1988); A. C. Bawa, C. S. Kim and A. D. Martin, Z. Phys. C **47**, 75 (1990); V. D. Barger, R. J. Phillips and D. P. Roy, Phys. Lett. B **324**, 236 (1994).
- [11] K. A. Assamagan, Y. Coadou and A. Deandrea, report ATL-COM-PHYS-2002-002, arXiv:hep-ph/0203121; P. Salmi, R. Kinnunen and N. Stepanov, arXiv:hep-ph/0301166.
- [12] K. A. Assamagan and Y. Coadou, Acta Phys. Polon. B **33**, 707 (2002); R. Kinnunen and A. Nikitenko, report CMS note 2003/006.
- [13] J. C. Collins and W. K. Tung, Nucl. Phys. B **278**, 934 (1986); M. A. Aivazis, J. C. Collins, F. I. Olness and W. K. Tung, Phys. Rev. D **50**, 3102 (1994); F. I. Olness and W. K. Tung, Nucl. Phys. B **308**, 813 (1988); M. Krämer, F. I. Olness and D. E. Soper, Phys. Rev. D **62**, 096007 (2000).
- [14] T. Plehn, Phys. Rev. D **67**, 014018 (2003).
- [15] E. Boos and T. Plehn, arXiv:hep-ph/0304034.
- [16] F. Maltoni, Z. Sullivan and S. Willenbrock, Phys. Rev. D **67**, 093005 (2003).
- [17] S. Dittmaier, M. Krämer and M. Spira, arXiv:hep-ph/0309204.
- [18] R. V. Harlander and W. B. Kilgore, Phys. Rev. D **68**, 013001 (2003).
- [19] S. H. Zhu, Phys. Rev. D **67**, 075006 (2003).
- [20] H. L. Lai *et al.* [CTEQ Collaboration], Eur. Phys. J. C **12**, 375 (2000).
- [21] see *e.g.* H. Baer, J. Ohnemus and J. F. Owens, Phys. Rev. D **40**, 2844 (1989) and Phys. Lett. B **234**, 127 (1990) and Phys. Rev. D **42**, 61 (1990); U. Baur, T. Han and J. Ohnemus, Phys. Rev. D **48**, 5140 (1993) and Phys. Rev. D **51**, 3381 (1995) and Phys. Rev. D **53**, 1098 (1996).
- [22] B. W. Harris and J. F. Owens, Phys. Rev. D **65**, 094032 (2002).
- [23] R. K. Ellis, D. A. Ross and A. E. Terrano, Nucl. Phys. B **178**, 421 (1981); Z. Kunszt and D. E. Soper, Phys. Rev. D **46**, 192 (1992); M. L. Mangano, P. Nason and G. Ridolfi, Nucl. Phys. B **373**, 295 (1992); S. Catani and M. H. Seymour, Nucl. Phys. B **485**, 291 (1997) [Erratum-ibid. B **510**, 503 (1997)]; S. Catani, S. Dittmaier, M. H. Seymour and Z. Trocsanyi, Nucl. Phys. B **627**, 189 (2002).
- [24] U. Baur and D. Zeppenfeld, Phys. Rev. Lett. **75**, 1002 (1995).
- [25] W. Beenakker, R. Höpker, M. Spira and P. M. Zerwas, Nucl. Phys. B **492**, 51 (1997); W. Beenakker, M. Klasen, M. Krämer, T. Plehn, M. Spira and P. M. Zerwas, Phys. Rev. Lett. **83**, 3780 (1999); A. Alves, O. Eboli and T. Plehn, Phys. Lett. B **558**, 165 (2003).
- [26] F. Borzumati, J. L. Kneur and N. Polonsky, Phys. Rev. D **60**, 115011 (1999).
- [27] E. L. Berger and H. Contopanagos, Phys. Lett. B **361**, 115 (1995); E. L. Berger and H. Contopanagos, Phys. Rev. D **54**, 3085 (1996); E. L. Berger and H. Contopanagos, Phys. Rev. D **57**, 253 (1998).
- [28] S. Catani, M. L. Mangano, P. Nason and L. Trentadue, Phys. Lett. B **378**, 329 (1996); R. Bonciani, S. Catani, M. L. Mangano and P. Nason, Nucl. Phys. B **529**, 424 (1998).
- [29] W. Beenakker, M. Krämer, T. Plehn, M. Spira and P. M. Zerwas, Nucl. Phys. B **515**, 3 (1998).
- [30] S. Narison, Phys. Lett. B **341**, 73 (1994).
- [31] E. L. Berger, M. Klasen and T. Tait, Phys. Lett. B **459**, 165 (1999); E. L. Berger, M. Klasen and T. M. P. Tait, Phys. Rev. D **62**, 095014 (2000); E. L. Berger, M. Klasen and T. M. P. Tait, Phys. Rev. D **67**, 099901 (2003).
- [32] E. L. Berger and J. W. Qiu, Phys. Rev. D **67**, 034026 (2003), and references therein.
- [33] L. J. Hall, R. Rattazzi and U. Sarid, Phys. Rev. D **50**, 7048 (1994); M. Carena, M. Olechowski, S. Pokorski and C. E. Wagner, Nucl. Phys. B **426**, 269 (1994); A. Belyaev, D. Garcia, J. Guasch and J. Sola, Phys. Rev. D **65**, 031701 (2002) [arXiv:hep-ph/0105053].
- [34] A. Belyaev, D. Garcia, J. Guasch and J. Sola, arXiv:hep-ph/0203031.
- [35] M. Carena, D. Garcia, U. Nierste and C. E. Wagner, Nucl. Phys. B **577**, 88 (2000); J. Guasch, P. Häfliger and M. Spira, arXiv:hep-ph/0305101.
- [36] B. C. Allanach *et al.*, in *Proc. of the APS/DPF/DPB Summer Study on the Future of Particle Physics (Snowmass 2001)* ed. N. Graf, Eur. Phys. J. C **25**, 113 (2002); N. Ghodbane and H. U. Martyn, in *Proc. of the APS/DPF/DPB Summer Study on the Future of Particle Physics (Snowmass 2001)* ed. N. Graf, arXiv:hep-ph/0201233.
- [37] M. Drees and S. P. Martin, arXiv:hep-ph/9504324; J. L. Feng, K. T. Matchev and T. Moroi, Phys. Rev. D **61**, 075005 (2000).